Supporting Information: Understanding TADF: a joint experimental and theoretical study of DMAC-TRZ

Rama Dhali, D.K. Andrea Phan Huu, Francesco Bertocchi, Cristina Sissa, Francesca Terenziani and Anna Painelli*

Department of Chemistry, Life Science and Environmental Sustainability, Parma University, 43124 Parma, Italy

E-mail: anna.painelli@unipr.it

Supporting Information Available

Contents

List of Figures

List of Tables

1 Experimental spectroscopic data

DMAC, TRZ and DMAC-TRZ were acquired from Merck, and used without further purification. Spectroscopic data were collected in solution using HPLC-grade solvents from Merck. Absorption spectra were recordered with a Perkin Elmer Lambda 650 spectrophotometer. Steady-state and time-resolved luminescence spectra (including anisotropy) were recordered

on dilute solutions (absorbance lower than 0.1) with a FLS1000 Edinburgh Fluorometer equipped with a gated PMT detector. Low-temperature measurements were collected on glassy matrices of 2MeTHF at 77K (the solvent was stored over molecular sieves for one night, and filtered before use), that were fastly cooled using an Oxford Instrument Optistat DN cryostat.

Table S1: Absorption maxima and molar extinction coefficient of DMAC-TRZ in different solvents

Compound	Solvent	$\lambda_{abs}[nm]$	Molar Extinction Coefficient [L mol^{-1}cm^{-1}]
DMAC-TRZ	Toluene	382	1990
	Chloroform	382	2180
	DMSO	385	2250

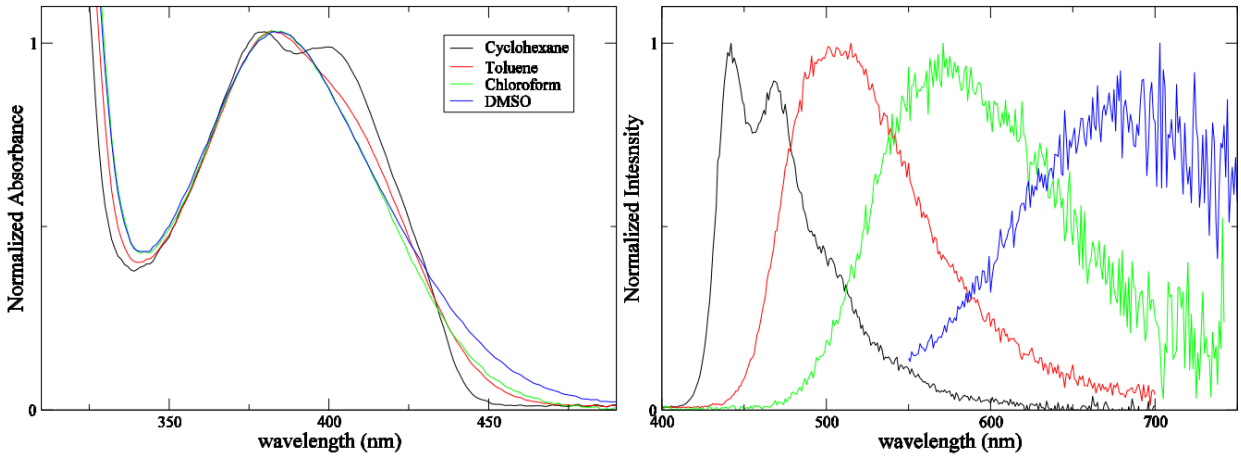

Figure S1: Steady state absorption (left panel) and emission spectra (right panel) of DMAC-TRZ in cyclohexane, toluene, chloroform and DMSO.

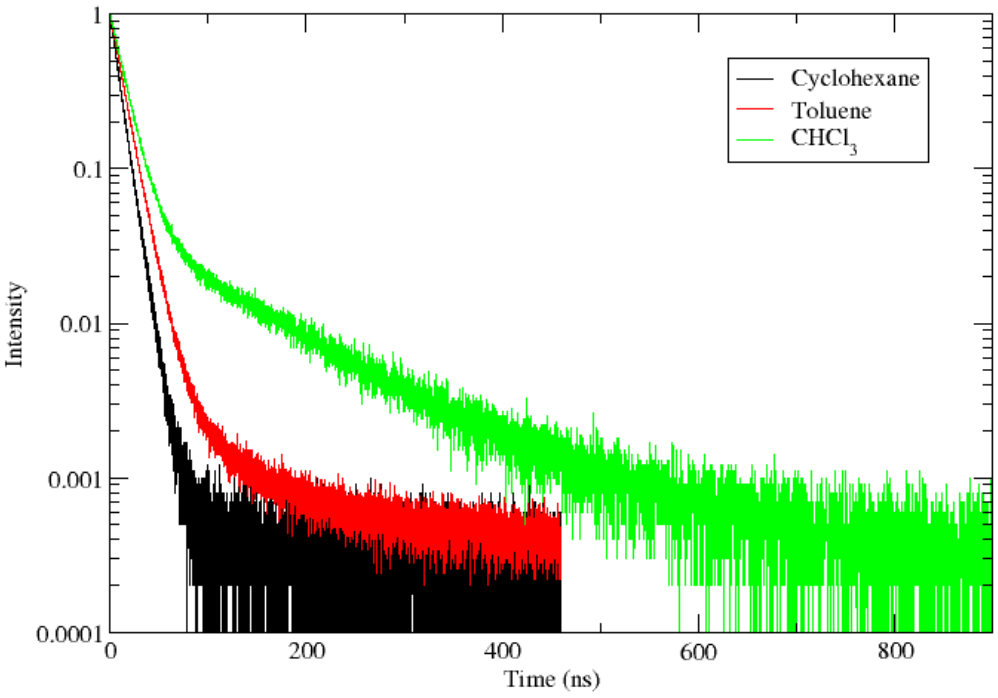

Figure S2: Fluorescence intensity (excitation 375 nm, detection at the maximum of emission for each solvent) vs time for DMAC-TRZ in different solvents.

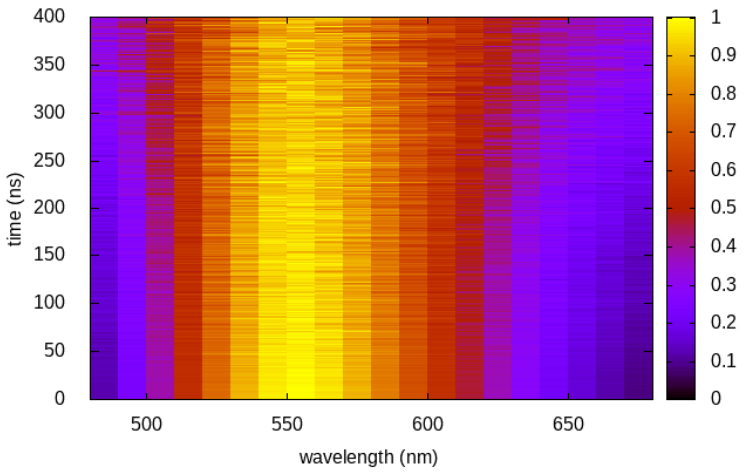

Figure S3: Time resolved emission spectra of DMAC-TRZ in chloroform.

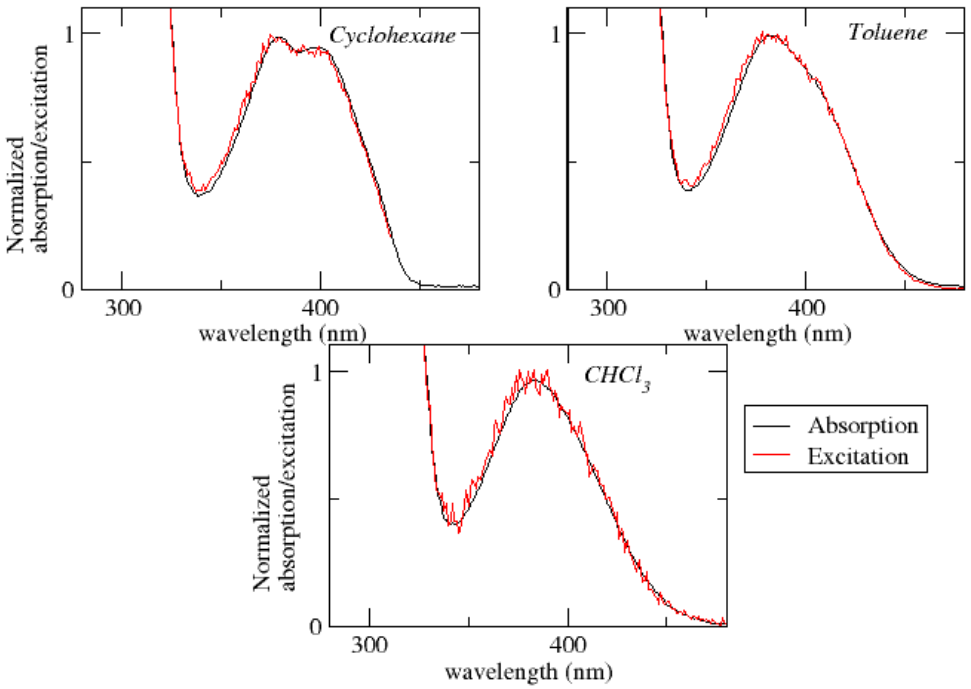

Figure S4: Absorption and fluorescence excitation spectra of DMAC-TRZ in different solvents.

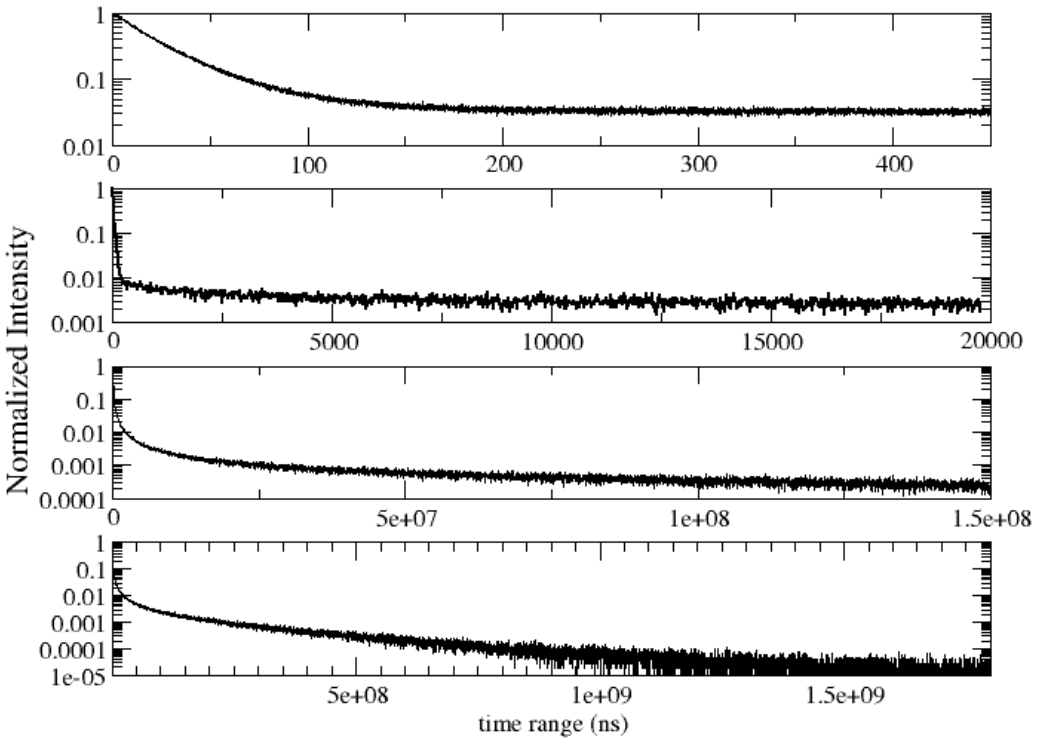

Figure S5: Fluorescence intensity (excitation: 405nm, emission 485nm) collected for DMAC-TRZ in 2MeTHF at 77K on different time ranges.

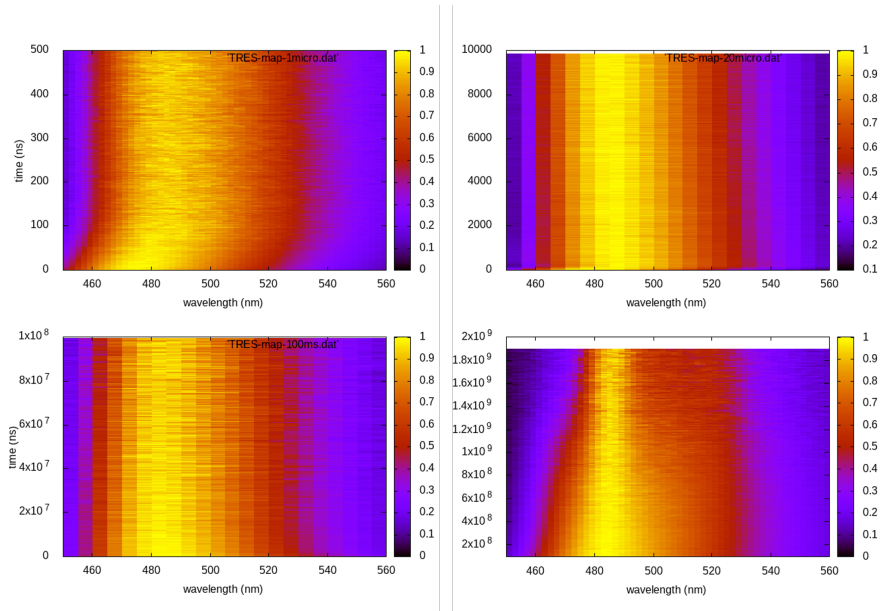

Figure S6: Time resolved emission spectra of DMAC-TRZ in 2-Me-THF at 77K in different time ranges.

2 Computational details

We used Gaussian 16 B.10[S1] for the DFT optimization of DMAC-TRZ ground state (B3LYP/6-31G(d)), then excited states are calulated in TD-DFT (Tamm-Dancoff approximation) using different functionals: B3LYP,[S2] CAM-B3LYP,[S3] M06-2X functionals[S4] and LC-ω*PBE.[S5] Spin-orbit coupling (SOC) in DMAC-TRZ is calculated using M06-2X/6-31G(d). All calculations are performed under TD-DFT within Tamm-Dancoff approximation. The default Breit-Pauli Hamiltonian is adopted to calculate SOC between TD-DFT states in Orca 4.1 package.[S6,S7] Avogadro[S8] was used as visualization tool.

2.1 Long range ω-tuned functional

TD-DFT calculations based on different functionals lead to wildly different results for the excitation spectrum of TADF dyes, particularly with reference to the ΔE_{ST} value and, more generally, in terms of relative order of CT and local excited (LE) states.[S9] Range-separated exchange functionals were suggested to solve the issue. In this approch, the range-separated parameter (ω) is optimally tuned to to get the exact exchange (eX) according to the interelectron distance, r_{12}:[S9]

$$\frac{1}{r_{12}} = \frac{1-[\alpha+\beta\,\mathrm{erf}(\omega\cdot r_{12})]}{r_{12}} + \frac{\alpha+\beta\,\mathrm{erf}(\omega\cdot r_{12})}{r_{12}} = SR + LR \tag{1}$$

where $erf(x) = \frac{2}{\sqrt{x}}\int_0^x exp(-t^2)dt$ and ω is range-tuning parameter.

The first term is the short-range (SR) component which is evaluated by DFT derived from local-density or generalized-gradient approximations. The second term is the long-range (LR) component which is evaluated by Hatree-Fock (HF). The α parameter quantifies the amount of eX in the SR limit, and $\alpha+\beta$ quantifies the amount of eX in the LR limit. The range-separation parameter ω defines the inverse distance at which exchange terms switch from DFT to HF. For any functional, $0 \leq \alpha \leq 1$, $0 \leq \beta \leq 1$ and $0 \leq \alpha+\beta \leq 1$. We use CAM-B3LYP ($\alpha = 0.19, \alpha+\beta = 0.65$), M06-2X (56% eX), B3LYP (20% eX) and

LC-ωPBE ($\alpha = 0, \alpha + \beta = 1$) for comparison.[S9,S10] By deafult LC-ωPBE has a ω value of 0.4 $Bohr^{-1}$.[S11,S12] Now we tune this parameter to get the optimal ω (ω^*) using LC-ωPBE functional.

Baer *et al.* proposed a nonempirical method to get optimal ω by enforcing Koopman's theorem,[S13] stating that the negative HOMO energy, $-\epsilon_H(N)$, of the N-electron system should be equal to the molecular vertical ionization potential, $IP(N)$.

$$-\epsilon_H^{\omega}(N) = IP^{\omega}(N) \tag{2}$$

Since, TADF molecules are donor-acceptor systems, it is useful to focus on ionization potential (related to donor component) as well as on electron affinity (related to acceptor component). The vertical electron affinity of N-electron system, $EA(N)$ should be equal to the negative energy of HOMO energy of anion system, $-\epsilon_H(N+1)$.

$$-\epsilon_H^{\omega}(N+1) = EA^{\omega}(N) \tag{3}$$

In optimal range-separated method, the goal is to minimize $J(\omega)$ defined as:

$$J(\omega) = |\epsilon_H^{\omega}(N) + IP^{\omega}(N)| + |\epsilon_H^{\omega}(N+1) + EA^{\omega}(N)| \tag{4}$$

We have performed our study using LC-ωPBE and found 19.5% as optimal ω for the ground state equlibrium structure. We find the optimal ω gives qualitatively similar result with M06-2X compared to CAM-B3LYP and B3LYP for relative position among LE and CT states.

Optimal ω is geometry dependent.[S14] The dihedral angle of ground state equilibrium structure is 90°. We calculated the optimal ω for dihedral angles of 75°, 60°, 45° and compare with other functionals. Optimal ω values are listed in Table S2 and plots for transition energy calculated for different dihedral angles and functionals are shown in Fig. S7.

Table S2: Optimal ω values estimated for different geometries

Dihedral angle	ω
90°	0.195
75°	0.195
60°	0.190
45°	0.185

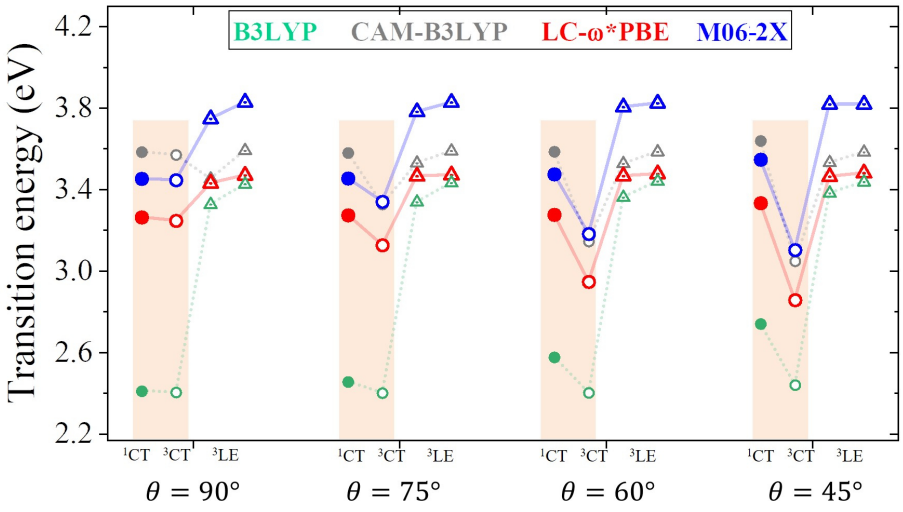

Figure S7: Excitation energies of the four lowest excited states calculated with different functionals and for different θ values.

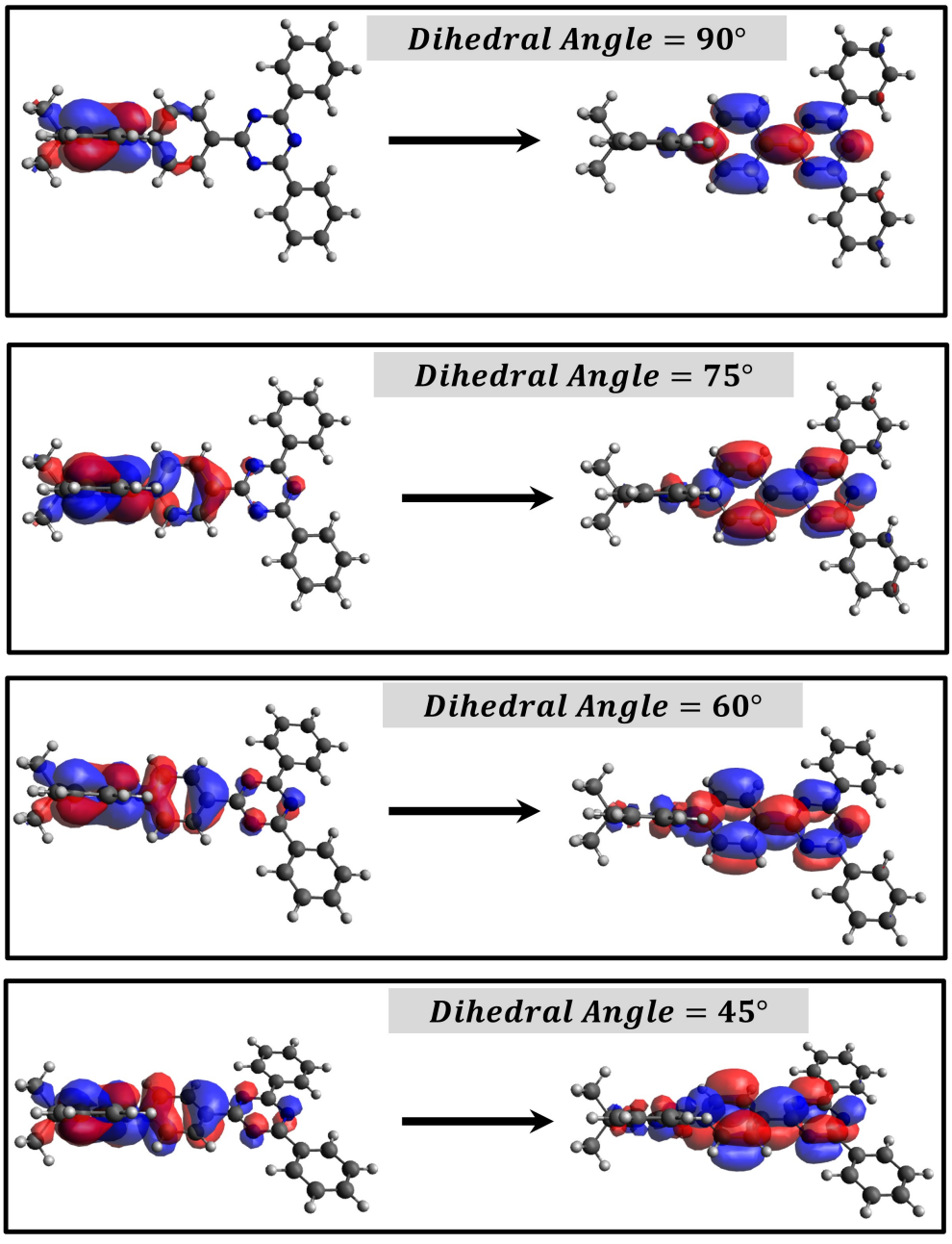

Figure S8: Natural transition orbitals calculated for T_1 state for different θ values.

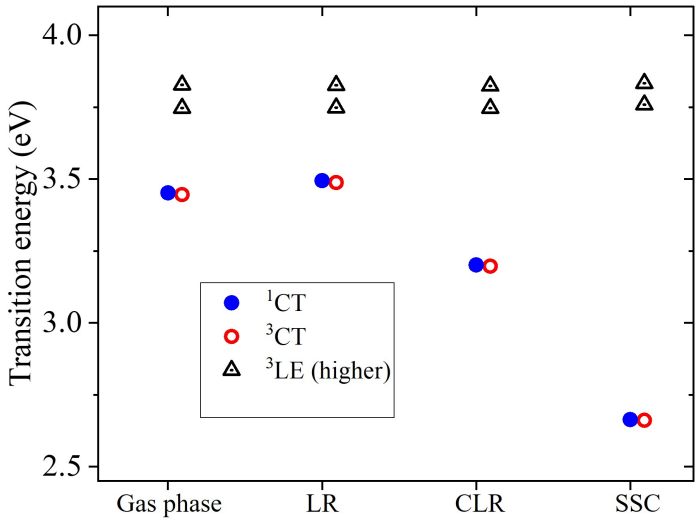

Figure S9: Excitation energies of the lowest singlet and three-lowest triplet states in gas phase and methylcyclohexane using different formalisms for solvent response: linear response (LR), corrected linear response (CLR) and state specific correction (SSC).[S15–S17]

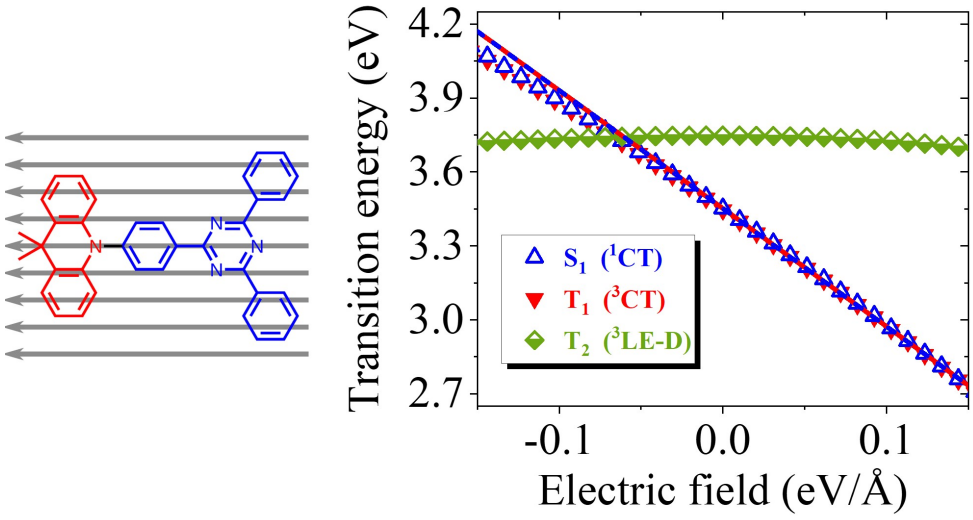

Figure S10: Left panel: a sketch of the molecule under an applied uniform electric field. Right panel: transition energies of the lowest singlet and triplet states as a function of an external electric field applied along the CT direction. Symbols refer to TD-DFT results, continuous lines show ESM energies for the CT states.

3 Model details

3.1 Three-state model for DMAC-TRZ

The three-state Hamiltonian reads (basis: $|N\rangle$, $|Z\rangle$, $|T\rangle$):

$$\hat{H} = \begin{pmatrix} 0 & -\tau_0|\sin\delta| & V_{soc} \\ -\tau_0|\sin\delta| & 2z & 0 \\ V_{soc} & 0 & 2z \end{pmatrix} + a_2\delta^2 + a_4\delta^4 \tag{5}$$

where all symbols are defined in the main text.

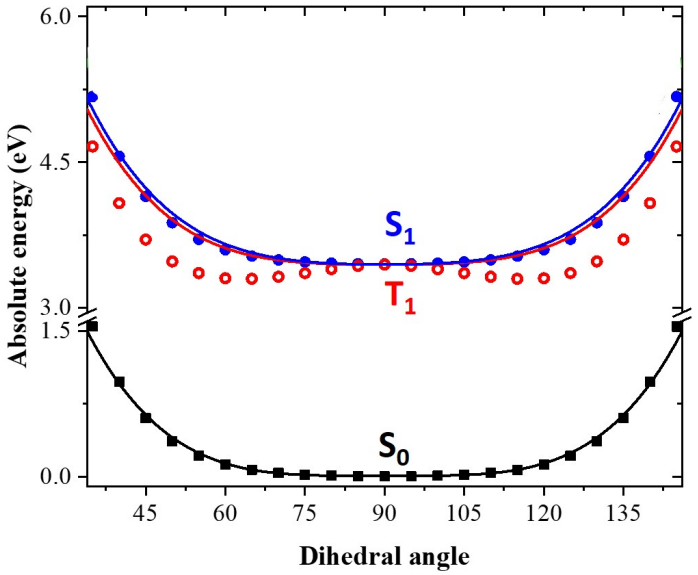

Figure S11: Energy of the ground and lowest excited singlet and triplet states calculated as a funcion of θ in TD-DFT (symbols) and three-state ESM (lines).

3.2 θ dependence of τ

System properties in ESMs are dependent on the ionicity ρ that is defined by the model parameters as:

$$\rho = \frac{1}{2}\left(1 - \frac{z}{\sqrt{z^2+\tau^2}}\right) \tag{6}$$

In particular the transition dipole moment, μ_{CT} is given by:

$$\mu_{CT} = \mu_0\sqrt{\rho(1-\rho)} \tag{7}$$

where μ_0 is the dipole moment associated to the zwitterionic state. The CT transition energy, $\hbar\omega_{CT}$

$$\hbar\omega_{CT} = \frac{\tau(\theta)}{\sqrt{\rho(1-\rho)}} \tag{8}$$

The product $\mu_{CT}\hbar\omega_{CT}$ has the same θ dependence as $\tau(\theta)$:

$$\mu_{CT}\hbar\omega_{CT} = \mu_0\tau(\theta) \tag{9}$$

The dependence of $\tau(\theta)$ is obtained fitting the values of $\mu_{CT}\hbar\omega_{CT}$ predicted using M06-2X/6-31G(d) calculations for different values of θ with the function $f(\theta) = A|\cos(\theta)|$ as in Fig. S12.

3.3 The role of the effective local triplet state

As stated in the main text, the choice of the effective local triplet (^{3}LE) state coupled to the CT triplet is somewhat arbitrary as it mimics the effects of several local triplet states. However, since we are interested in the properties of T_1, the lowest triplet, adopting different choices for the effective state has marginal effects on molecular and spectroscopic properties we are interested in. Specifically, Fig. S13 show the θ-dependence of the energies of the relevant states, of the singlet-triplet gap and spin-orbit coupling and of the weight of the

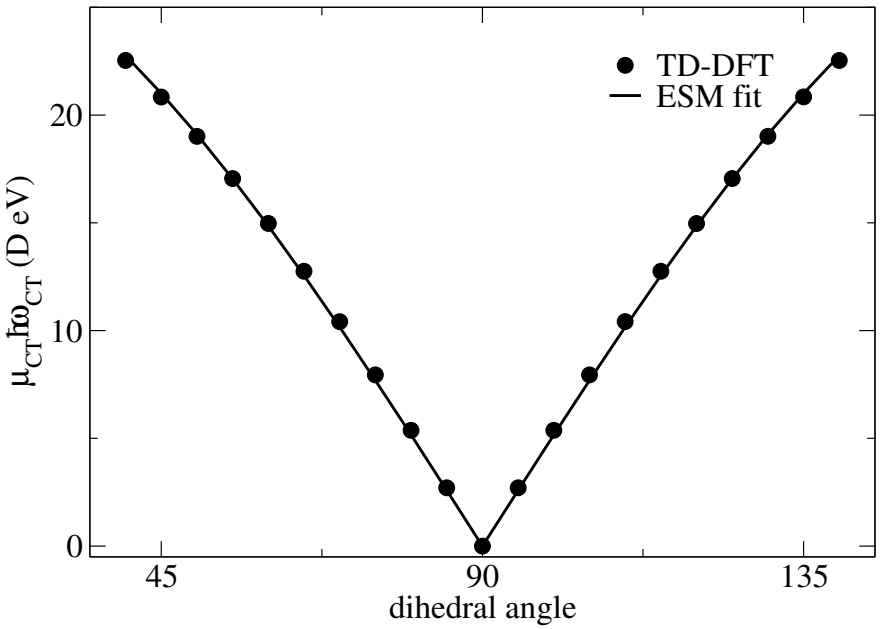

Figure S12: TD-DFT results for $\mu_{CT}\hbar\omega_{CT}$ (symbols) fitted with the function $A|\cos\theta|$ (line) with A as fitting parameter.

CT state in T_1 obtained adopting three different choices for the parametrization of the local triplet state, as reported in Table S3. The left panels in the Figure showing results for Model 1 coincide with data reported in the main text (Fig. 3). Middle panels refer to Model 2, where the energy and the coupling strength of the effective local triplet state are increased. Finally the rightmost column show results obtained for Model 3 that considers two coupled local triplets.

3.4 Determination of ϵ_v

The vibrational relaxation energy, ϵ_v, is estimated through DFT energy calculations on the isolated donor (D) and acceptor (A) and the respective ionized species, D^+ and A^-:

$$\epsilon_v = \left(E_{D^+}^{(D)} + E_{A^-}^{(A)}\right) - \left(E_{D^+}^{(D^+)} + E_{A^-}^{(A^-)}\right)$$

where $E_i^{(j)}$ is the energy of i in in the equilibrium structure of j (See Table S4). Calculations involving the open-shell systems D^+ and A^- were used unrestricted M06-2X/6-31G(d).

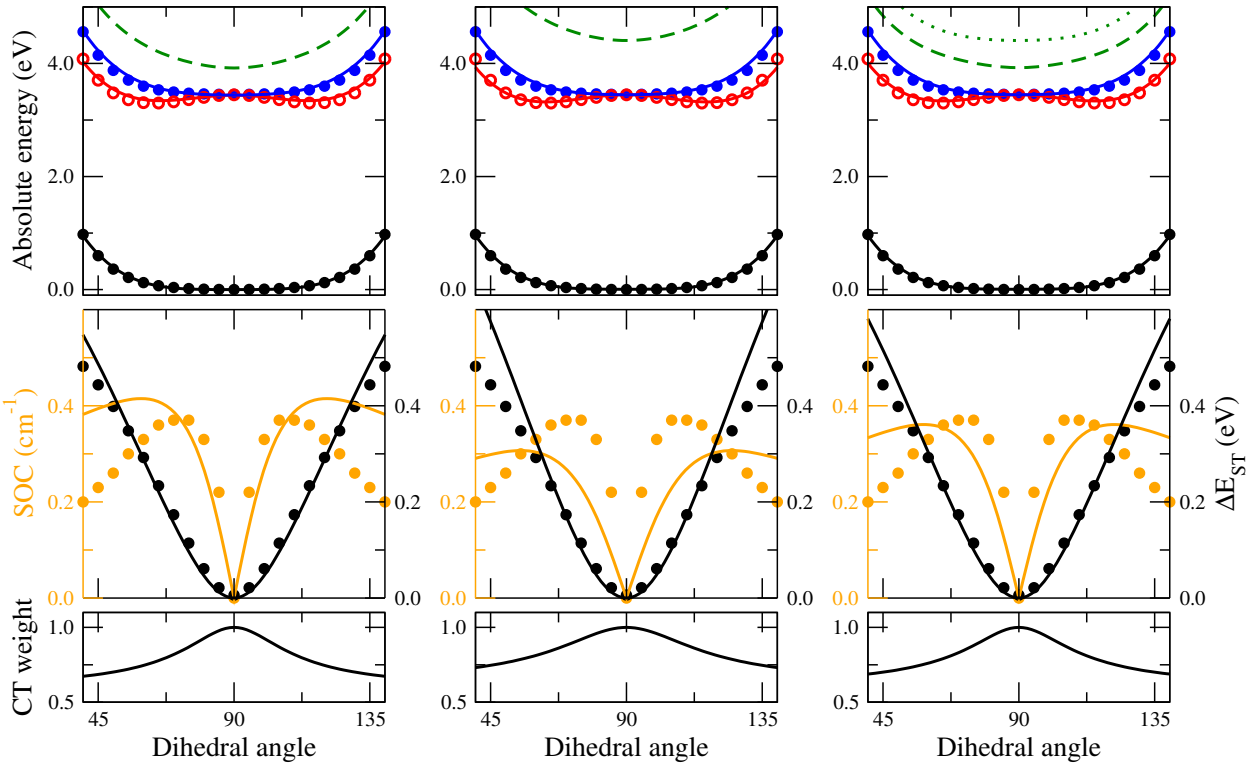

Figure S13: From top to bottom: PES, singlet triplet energy gap and spin-orbit coupling and the weight of the CT triplet in T_1 state. Left: Model 1 parametrization (see Table S3); middle: model 2; right: model 3.

Table S3: Different parametrizations of the model prosposed in the main text. Model 1 is the same parametrization as in main text Table 2. Model 2 is a different parametrization, obtained for a different energy of $|L\rangle$. Model 3 accounts for an additional local state $|L'\rangle$ that is coupled through the following matrix elements: $\langle L'|\,\hat{H}\,|T\rangle = -\beta_0'|\sin(\delta)|$ and $\langle L'|\,\hat{H}\,|Z\rangle = W_{soc}'$.

	Model 1	Model 2	Model 3
z (eV)	1.72	1.72	1.72
τ_0 (eV)	0.75	0.75	0.75
k (eV)	1.96	2.20	1.96
β_0 (eV)	0.85	1.20	0.75
k' (eV)	-	-	2.20
β_0' (eV)	-	-	0.60
a_2 (eV)	$6.00{\cdot}10^{-5}$	$6.00{\cdot}10^{-5}$	$6.00{\cdot}10^{-5}$
a_4 (eV)	$1.43{\cdot}10^{-7}$	$1.43{\cdot}10^{-7}$	$1.43{\cdot}10^{-7}$
V_{soc} (cm^{-1})	3.10	3.10	3.10
W_{soc} (cm^{-1})	1.40	1.40	1.00
W_{soc}' (cm^{-1})	-	-	1.00

Table S4: SCF energies of D^+ and A^- used to estimate ϵ_v.

	SCF Energy (a.u.)
$E_{D^+}^{(D)}$	-634.873448021
$E_{D^+}^{(D^+)}$	-634.875775452
$E_{A^-}^{(A)}$	-973.174499157
$E_{A^-}^{(A^-)}$	-973.178453857

3.5 Modelling the solvent response

The total (solute+solvent) Hamiltonian is $\hat{\mathcal{H}}_{tot} = \hat{\mathcal{H}}_{sys} + \hat{\mathcal{H}}_{sol}$. In ESMs we take into account electrostatic interactions between the solute treated as a point dipole, and the solvent treated as a dielectric continuum medium that hosts the solute in a cavity of radius a_0. The solvent responds to the solute generating an electric field, also called reaction field, F_r, proportional to the electric dipole moment of the solute.

Two regimes must be discriminated for the solvent response: (i) the response associated with electronic degrees of freedom is very fast and can be treated in the antiadiabatic approximation; (ii) the response associated with orientational degrees of freedom of polar solvent molecules is very slow and can be treated in the adiabatic approximation. So, the reaction field splits in two terms: $F_r = r_{el}\langle\mu\rangle + r_{or}\langle\mu\rangle$ where r_{el} and r_{or} are dependent on the cavity radius, the refractive index $\eta = \sqrt{\epsilon_{opt}}$ and the static dielectric constant (ϵ_{st}). Specifically, $r_{el} = \frac{2}{4\pi\epsilon_0 a_0^3} f(\epsilon_{opt})$ and $r_{or} = \frac{2}{4\pi\epsilon_0 a_0^3}(f(\epsilon_{st}) - f(\epsilon_{opt}))$ where $f(\epsilon) = \frac{\epsilon-1}{2\epsilon+1}$. We consider the solvent as an elastic medium so that a quadratic potential energy is associated to the two components of the reaction field, the relevant force constant being fixed to $1/(2r_{or/el})$ enforcing the proportionality between the reaction field and the molecular dipole moment at the equilibrium.

Adopting the adiabatic approximation to polar solvation and the antiadiabatic approximation for th electronic solvation, the Hamiltonian for the solvated molecule reads: $\hat{\mathcal{H}}_{tot} = \hat{\mathcal{H}}_{sys} - \frac{r_{el}}{2}\hat{\mu}^2 - F_{or}\hat{\mu} + \frac{1}{2r_{or}}F_{or}^2$, that, for the specific essential state model adopted for DMAC-

TRZ reduces to the Hamiltonian in Eq. 3 main text. The required dielectric parameters for the solvents are taken from the literature (except for 2MeTHF at 77K) and are listed in Table S5. Literature data for ϵ_{st} and ϵ_{opt} of glassy 2MeTHF at 77 K are not available. Since the refractive index of organic solvents increases linearly as the temperature decreases,,[S18] we set $\epsilon_{opt}^{\mathrm{2MeTHF}}(77K) = 2.016$. As for the static dielectric constant, the effective polarity of 2MeTHF increases as the temperature decreases and, for glassy 2MeTHF at 77K it is comparable to that of liquid EtOH or DMF,[S19] so we set $\epsilon_{st}^{\mathrm{2MeTHF}}(77K) = 30.5$.

Table S5: Solvent dielectric properties at ambient conditions.

solvent	ϵ_{opt}	ϵ_{st}
Cyclohexane	2.03	2.03
Toluene	2.24	2.38
Chloroform	2.09	4.81
2MeTHF	1.98	6.97

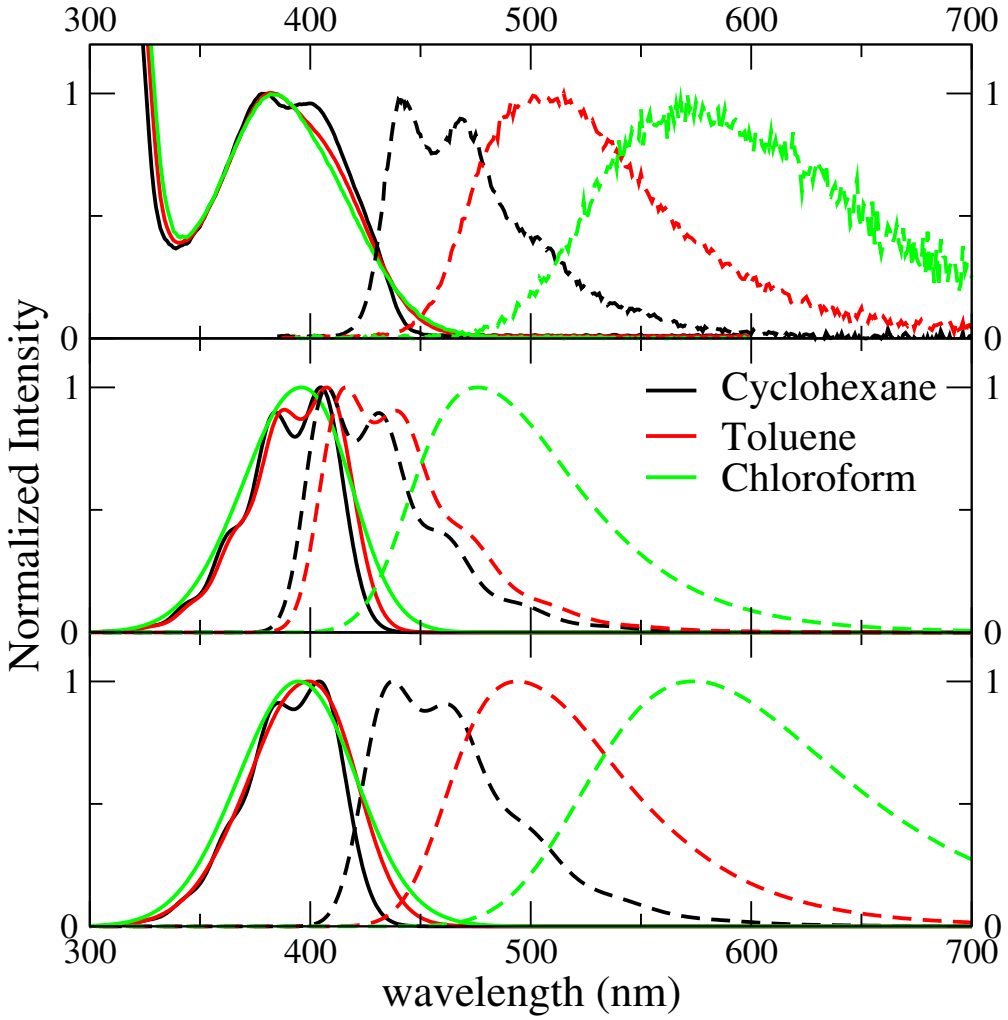

Figure S14: Normalized absorption and fluorescence spectra (continuous and dashed lines, respectively) of DMAC-TRZ in different solvents. Top panel: experimental data as in Fig. 1, main text. Middle panel: calculated spectra with ϵ_{or} estimated as described in the main text (same data as in Fig. 4, main text). Bottom panel: calculated spectra (298 K) adjusting ϵ_{or} as free fitting parameter: ϵ_{or}(Cyclohexane)=0.10 eV; ϵ_{or}(Toluene)=0.22 eV; ϵ_{or}(Cholorform)=0.40 eV. The HWHM associated to each transition is $\Gamma = 0.03$ eV.

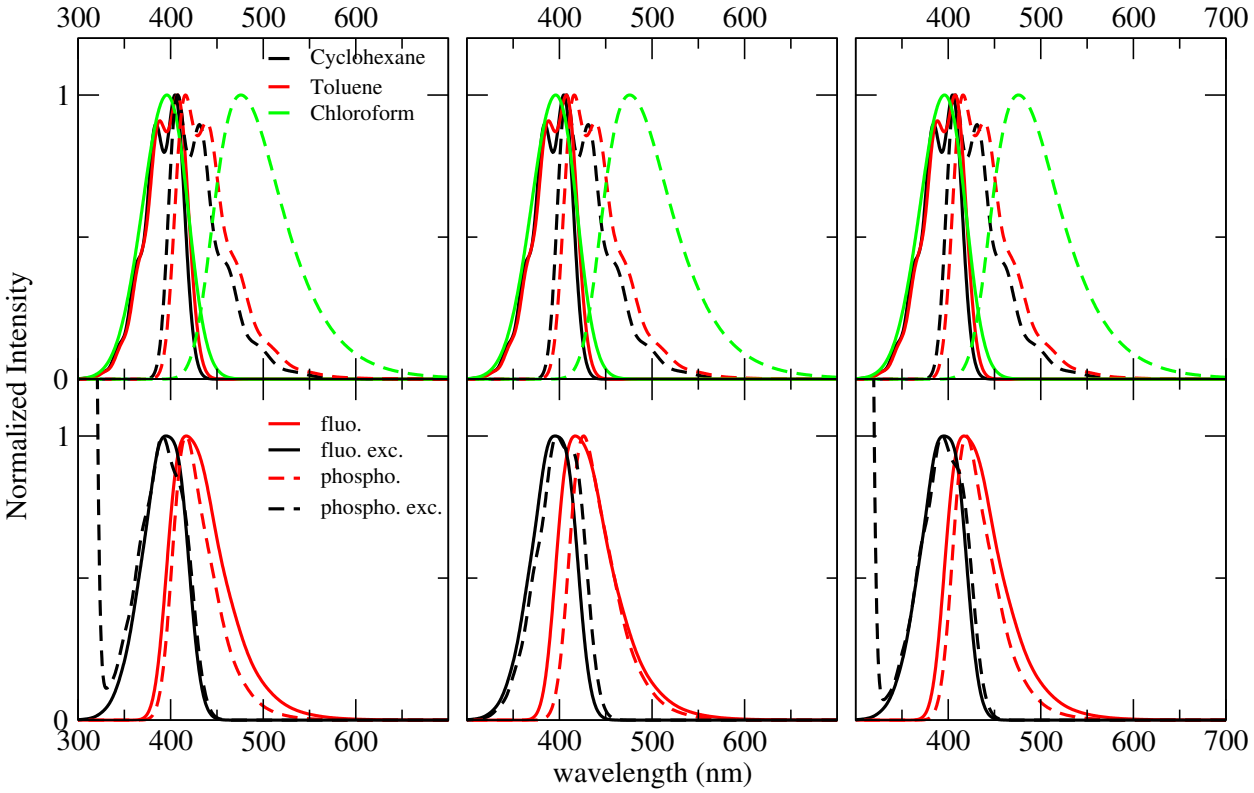

Figure S15: Top: Normalized absorption and fluorescence spectra (continuous and dashed lines, respectively) of DMAC-TRZ in different solvents. Bottom: emission and excitation spectra of DMAC-TRZ in glassy 2MeTHF. The columns show spectra calculated for model parameters listed in Table S3 (from left to right: model 1 to 3).

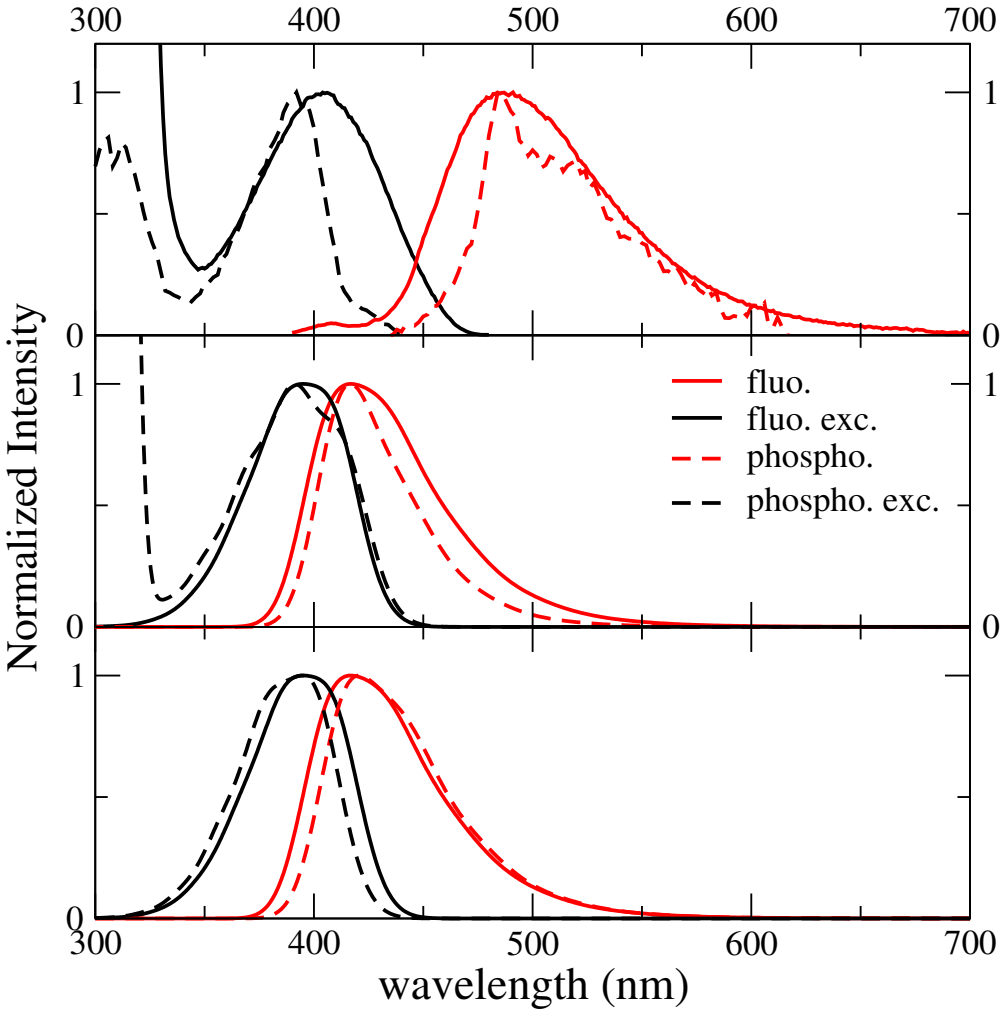

Figure S16: Emission and excitation spectra of DMAC-TRZ in frozen 2MeTHF. Top panel: experimental spectra as in Fig. 1, main text. Middle panel: calculated spectra as in Fig. 4(b) main text. Bottom panel: the same as in the middle panel, but with phosphorescence spectra calculated only accounting for the contribution from the CT state.

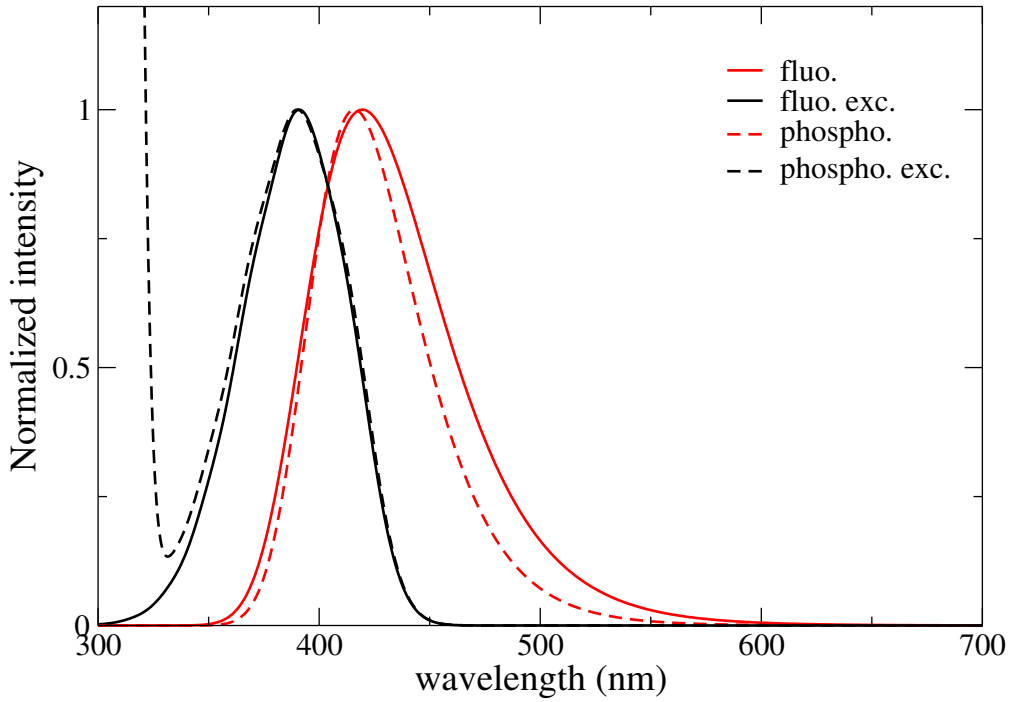

Figure S17: Calculated emission and excitation spectra of DMAC-TRZ in matrix with the same dielectric properties of 2-MeTHF at RT. Continuous lines: fluorescence and fluorescence excitation spectra. Dashed lines: phosphorescence and phosphorescence excitation spectra. Excitation spectra are computed setting the excitation wavelength as the wavelength of the maximum of the respective emission (fluroescence or phosphorescence) spectra.

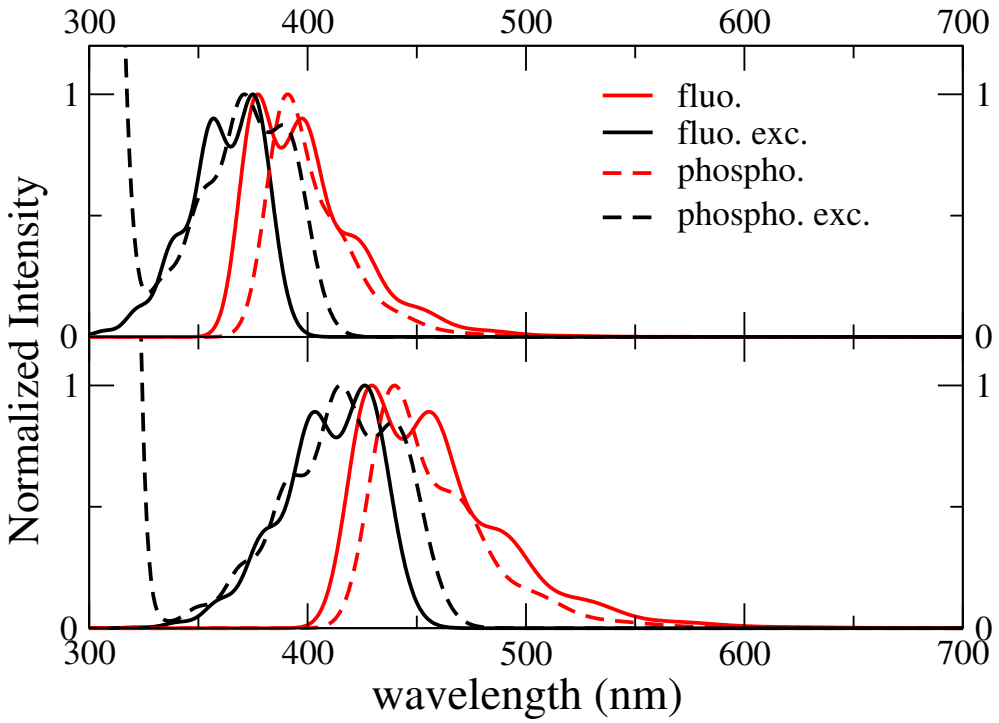

Figure S18: Calculated emission and excitation spectra of DMAC-TRZ in a $\eta = 1$ matrix (top) and in a $\eta = 2$ matrix (bottom) at 298 K. Continuous lines: fluorescence and fluorescence excitation spectra. Dashed lines: phosphorescence and phosphorescence excitation spectra. Excitation spectra are computed setting the excitation wavelength as the wavelength of the maximum of the respective emission (fluroescence or phosphorescence) spectra.

References

(S1) Frisch, M. J.; Trucks, G. W.; Schlegel, H. B.; Scuseria, G. E.; Robb, M. A.; Cheeseman, J. R.; Scalmani, G.; Barone, V.; Petersson, G. A.; Nakatsuji, H.; Li, X.; Caricato, M.; Marenich, A. V.; Bloino, J.; Janesko, B. G.; Gomperts, R.; Mennucci, B.; Hratchian, H. P.; Ortiz, J. V.; Izmaylov, A. F.; Sonnenberg, J. L.; Williams-Young, D.; Ding, F.; Lipparini, F.; Egidi, F.; Goings, J.; Peng, B.; Petrone, A.; Henderson, T.; Ranasinghe, D.; Zakrzewski, V. G.; Gao, J.; Rega, N.; Zheng, G.; Liang, W.; Hada, M.; Ehara, M.; Toyota, K.; Fukuda, R.; Hasegawa, J.; Ishida, M.; Nakajima, T.; Honda, Y.; Kitao, O.; Nakai, H.; Vreven, T.; Throssell, K.; Montgomery, J. A., Jr.; Peralta, J. E.; Ogliaro, F.; Bearpark, M. J.; Heyd, J. J.; Brothers, E. N.; Kudin, K. N.; Staroverov, V. N.; Keith, T. A.; Kobayashi, R.; Normand, J.; Raghavachari, K.; Rendell, A. P.; Burant, J. C.; Iyengar, S. S.; Tomasi, J.; Cossi, M.; Millam, J. M.; Klene, M.; Adamo, C.; Cammi, R.; Ochterski, J. W.; Martin, R. L.; Morokuma, K.; Farkas, O.; Foresman, J. B.; Fox, D. J. GaussianËIJ16 Revision B.01. 2016; Gaussian Inc. Wallingford CT.

(S2) Becke, A. D. Density-functional thermochemistry. III. The role of exact exchange. *The Journal of Chemical Physics* **1993**, *98*, 5648–5652.

(S3) Yanai, T.; Tew, D. P.; Handy, N. C. A new hybrid exchange-correlation functional using the Coulomb-attenuating method (CAM-B3LYP). *Chemical Physics Letters* **2004**, *393*, 51 – 57.

(S4) Zhao, Y.; Truhlar, D. G. The M06 suite of density functionals for main group thermochemistry, thermochemical kinetics, noncovalent interactions, excited states, and transition elements: two new functionals and systematic testing of four M06-class functionals and 12 other functionals. *Theoretical Chemistry Accounts* **2008**, *120*, 215–241.

(S5) Sun, H.; Zhong, C.; Brédas, J.-L. Reliable Prediction with Tuned Range-Separated Functionals of the Singlet-Triplet Gap in Organic Emitters for Thermally Activated Delayed Fluorescence. *Journal of Chemical Theory and Computation* **2015**, *11*, 3851–3858, PMID: 26574466.

(S6) Neese, F. The ORCA program system. *WIREs Computational Molecular Science* **2012**, *2*, 73–78.

(S7) Neese, F. Efficient and accurate approximations to the molecular spin-orbit coupling operator and their use in molecular g-tensor calculations. *The Journal of Chemical Physics* **2005**, *122*, 034107.

(S8) Hanwell, M. D.; Curtis, D. E.; Lonie, D. C.; Vandermeersch, T.; Zurek, E.; Hutchison, G. R. Avogadro: an advanced semantic chemical editor, visualization, and analysis platform. *Journal of Cheminformatics* **2012**, *4*, 17.

(S9) Sun, H.; Zhong, C.; Brédas, J.-L. Reliable Prediction with Tuned Range-Separated Functionals of the Singlet-Triplet Gap in Organic Emitters for Thermally Activated Delayed Fluorescence. *Journal of Chemical Theory and Computation* **2015**, *11*, 3851–3858, PMID: 26574466.

(S10) Nguyen, K. A.; Day, P. N.; Pachter, R. The performance and relationship among range-separated schemes for density functional theory. *The Journal of Chemical Physics* **2011**, *135*, 074109.

(S11) Vydrov, O. A.; Scuseria, G. E. Assessment of a long-range corrected hybrid functional. *The Journal of Chemical Physics* **2006**, *125*, 234109.

(S12) Raeber, A. E.; Wong, B. M. The Importance of Short- and Long-Range Exchange on Various Excited State Properties of DNA Monomers, Stacked Complexes, and Watson-Crick Pairs. *Journal of Chemical Theory and Computation* **2015**, *11*, 2199–2209, PMID: 26574420.

(S13) Kronik, L.; Stein, T.; Refaely-Abramson, S.; Baer, R. Excitation Gaps of Finite-Sized Systems from Optimally Tuned Range-Separated Hybrid Functionals. *Journal of Chemical Theory and Computation* **2012**, *8*, 1515–1531, PMID: 26593646.

(S14) Eng, J.; Laidlaw, B. A.; Penfold, T. J. On the geometry dependence of tuned-range separated hybrid functionals. *Journal of Computational Chemistry* **2019**, *40*, 2191–2199.

(S15) Cammi, R.; Mennucci, B. Linear response theory for the polarizable continuum model. *The Journal of Chemical Physics* **1999**, *110*, 9877–9886.

(S16) Caricato, M.; Mennucci, B.; Tomasi, J.; Ingrosso, F.; Cammi, R.; Corni, S.; Scalmani, G. Formation and relaxation of excited states in solution: A new time dependent polarizable continuum model based on time dependent density functional theory. *The Journal of Chemical Physics* **2006**, *124*, 124520.

(S17) Improta, R.; Barone, V.; Scalmani, G.; Frisch, M. J. A state-specific polarizable continuum model time dependent density functional theory method for excited state calculations in solution. *The Journal of Chemical Physics* **2006**, *125*, 054103.

(S18) Piñeiro, Á.; Brocos, P.; Amigo, A.; Pintos, M.; Bravo, R. Refractive Indexes of Binary Mixtures of Tetrahydrofuran with 1-Alkanols at 25°C and Temperature Dependence of n and ρ for the Pure Liquids. *Journal of Solution Chemistry* **2002**, *31*, 369–380.

(S19) Bublitz, G. U.; Boxer, S. G. Effective Polarity of Frozen Solvent Glasses in the Vicinity of Dipolar Solutes. *Journal of the American Chemical Society* **1998**, *120*, 3988–3992.